Kim, J-S., Larrosa, N. O., Horn, A. J., Kim, Y-J., & Ainsworth, R. A. (2017). Notch bluntness effects on fracture toughness of a modified S690 steel at 150 °C. *Engineering Fracture Mechanics*. https://doi.org/10.1016/j.engfracmech.2017.05.047

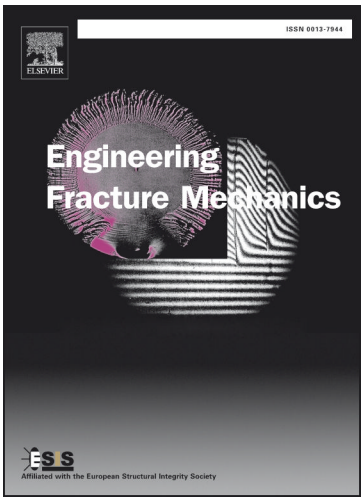

Notch Bluntness Effects on Fracture Toughness of A Modified S690 Steel at 150°C

J.-S. Kim, N.O. Larrosa, A.J. Horn, Y.-J. Kim, R.A. Ainsworth

PII: S0013-7944(16)30497-0
DOI: http://dx.doi.org/10.1016/j.engfracmech.2017.05.047
Reference: EFM 5574

To appear in: *Engineering Fracture Mechanics*

Received Date: 18 October 2016
Revised Date: 17 May 2017
Accepted Date: 22 May 2017

Please cite this article as: Kim, J.-S., Larrosa, N.O., Horn, A.J., Kim, Y.-J., Ainsworth, R.A., Notch Bluntness Effects on Fracture Toughness of A Modified S690 Steel at 150°C, *Engineering Fracture Mechanics* (2017), doi: http://dx.doi.org/10.1016/j.engfracmech.2017.05.047

NOTCH BLUNTNESS EFFECTS ON FRACTURE TOUGHNESS OF A MODIFIED S690 STEEL AT 150^{O}C

J-S Kim*[1], N O Larrosa[2], A J Horn[3] Y-J Kim[1] and R A Ainsworth[4]

1. Department of Mechanical Engineering, Korea University
Anam-Dong, Seongbuk-Gu
Seoul 136-701, South Korea
2. School of Materials, The University of Manchester
Manchester M13 9PL, UK
3. Clean Energy Europe - Nuclear Services, Amec Foster Wheeler
Warrington WA3 6XF, UK
4. School of Mechanical, Aerospace & Civil Engineering, The University of Manchester
Manchester M13 9PL, UK

* Corresponding author, email: nicolas.larrosa@manchester.ac.uk (N O Larrosa)

ABSTRACT

This paper addresses the effect of blunt defects on the structural integrity assessment of steels. Smooth tensile, notched bar tensile and multi-specimen single edge notched bend tests with various notch acuities have been performed and show an increase in effective ductile fracture toughness with increasing notch radius. A ductile fracture model has been shown to be capable of predicting the specimen responses including the local variation of ductile crack extension through the thickness. An empirical fit developed to describe the effect of notch radius on cleavage fracture toughness has been examined and found to be also capable of describing the effect of notch radius on ductile fracture toughness.

KEYWORDS: Blunt notch; Failure assessment diagram; Defect assessment; Ductile fracture model; Effective fracture toughness

NOMENCLATURE

a	crack size
a_o	initial crack length
A_{pl}	plastic component of the area under the load-LLD curve
b	remaining ligament
B	specimen thickness
E	elastic modulus
$f\left(a/W\right)$	stress intensity factor function
J	J-integral
J_{el}^{ρ}	J value evaluated elastically for a blunt defect
$J_{0.2}^{\rho=0.15}$	J value at 0.2mm crack growth for an acute notch (effectively a sharp crack)
$J_{0.2}^{\rho}$	J value at 0.2mm crack growth for a blunt defect
K_I^{ρ}	mode I stress intensity factor for a blunt defect
K_{mat}	fracture toughness
K_{mat}^{ρ}	fracture toughness for a blunt defect
K_r	fracture ratio in FAD
L_r	load to collapse load ratio in FAD
L_e	size of damage element
P	applied load
P_L	(plastic) limit load of a structure containing a defect
R	notch radius in tensile specimen
S	loading span of SE(B) specimen
U_P	plastic component of the area under the load-LLD curve
W	specimen width
Y	stress intensity factor function
α, β, γ	material constants

Δa	average ductile crack growth
$\Delta\varepsilon_e^p$	incremental equivalent plastic strain
ε_f	fracture strain
γ_{pl}	correction factor in ASTM formula for calculating J
ϕ, ℓ	material constants describing notch stress effect on toughness
η_p	factor in BS formula for calculating J
η_{pl}	factor in ASTM formula for calculating J
ρ	notch root radius in SE(B) specimens
σ_{YS}	0.2% proof stress
σ_e	von Mises effective stress
σ_m/σ_e	stress triaxiality
σ_m	hydrostatic stress
σ_N	elastic notch stress
$\sigma_1, \sigma_2, \sigma_3$	principal stresses
ν	Poisson's ratio
ω, $\Delta\omega$	accumulated damage and incremental damage, respectively

Subscript

i	denotes instantaneous value of crack size or load

Abbreviations

2-D, 3-D	two-dimensional, three-dimensional
ASTM	American Society for Testing and Materials
BS	British Standards
ESIS	European Structural Integrity Society
C(T)	compact tension
FAD	failure assessment diagram
FE	finite element
J-R	fracture resistance in terms of J versus Δa
LLD	load-line displacement
SE(B)	single edge notched bend
TES	twice-elastic slope

1. INTRODUCTION

A source of uncertainty and conservatism is the value of fracture toughness (K_{mat}) that is used in structural integrity assessments procedures, such as API579 [1], BS7910 [2] and R6 [3]. For conservative assessments, the value of K_{mat} is commonly derived from deeply cracked specimens, such as standard compact tension, C(T), or single edge notch bend, SE(B), specimens. High constraint conditions near the crack tip are ensured in such specimens and this corresponds to lower-

bound toughness values independent of specimen size and geometry. In practice many defects formed during manufacture or in service are not sharp [4, 5] and for such defects the local elastic-plastic stress and strain fields are known to be less severe than those at the tip of a sharp crack, resulting in an increased capacity to sustain load and, thus, higher toughness.

A number of experimental studies have examined specimens containing non-sharp defects in order to evaluate the effective fracture toughness for a variety of materials and notch geometries. Cleavage fracture data [6, 7], ductile initiation and tearing data [8-11] and the influence of notch geometry on the fracture mechanism [12-14] have been reported.

Experimental evaluation of the effective fracture toughness is, however, expensive and time-consuming. Some authors [15-19] have therefore proposed simplified global approaches, essentially based on one- or two-parameter linear elastic or elastic–plastic fracture mechanics, to evaluate a notch driving force and therefore the effect of the notch radius on specimen or component fracture response. Alternatively, more recently, the current authors have used a local approach to fracture to predict the effect of notch acuity [20] and low constraint conditions [21] on ductile fracture toughness. Local approaches are based on local fracture criteria established from a small number of tests typically carried out on notched specimens.

The local approach methodology presented in [20] was purely numerical. The present paper attempts to provide validation of this local approach. First, Section 2 presents the results of tensile tests and multi-specimen ductile tearing tests on specimens with a range of notch radius. Then Section 3 describes how the finite element local approach methodology of [20] has been calibrated and applied to the material and specimens presented in Section 2. Section 4 compares the numerical results with the experimental data for a range of notch radius. How the results can be included in modified fitness-for-service methods to allow for notch bluntness is discussed in Section 5 before the paper closes with conclusions in Section 6.

2. Experiments

The material used for this study of the effects of notch bluntness on ductile fracture properties was a structural steel grade S690, which has a specified minimum yield strength of 690MPa at room temperature. However, the steel was specially heat treated to make fracture occur by cleavage at room temperature and cleavage fracture results have been reported in [19]. Therefore, for the ductile tests it was necessary to adopt a test temperature of 150°C to ensure a fully ductile response. Smooth and notched bar tensile tests were performed as described in Section 2.1. The single edge notched bend, SE(B), tests with various notch acuities are described in Section 2.2. A summary of the tests is given in Table 1.

2.1 Tensile test data

Standard smooth round bar specimens used in tensile test were designed in accordance with ASTM E8/E8M [22]. The gauge length and the cross-sectional area of the gauge section of the specimens were 75mm and 100mm^2, respectively. Fig. 1 shows the engineering stress-strain curves of the

modified S690 steel from two smooth tensile tests. The average tensile properties derived from the smooth bar tensile tests are presented in Table 2.

Fig. 2 shows the geometry of the double notched bar specimens. The gauge length and the distance between the notches are 94mm and 30mm, respectively. The diameters of the gauge section and notched section are 11mm and 6mm, respectively. Three different notch radii, R = 1.2mm, 2.0mm and 6.4mm were used to obtain the fracture strain for the different states of stress triaxiality. Each notched tensile specimen contained two notches and the diametrical contraction was measured at both notches. The test results are presented as load versus diametral contraction of the failed notch as shown in Fig 3. The yield load and maximum tensile load of the notched specimens decreased with increasing notch radius whereas the ductility of the specimens increased with increasing notch radius.

2.2 SE(B) test data

Fig. 4 shows the geometry of the SE(B) tests. The SE(B) specimens had a square cross-section (12.5x12.5mm) without side grooves and a blunt notch of depth 6.2mm, including the notch radius. The notches were machined with a semi-circular shaped notch of radius, ρ = 0.15mm, 0.25mm, 0.75mm, 1.2mm or 2.0mm. The notches were machined using electro-discharge machining for the specimens with ρ = 0.15mm, 0.25mm and 0.75mm; larger radius notches were machined using a cutting wheel. The span of the three-point bend rig is 50mm, which is four times the width of the specimen.

The SE(B) tests were performed at 150^{o}C to ensure a ductile response and stopped at displacements generally in excess of the displacement at the maximum load point, as illustrated in Fig. 5(a). During each test, the load applied to the roller was recorded and also the notch mouth opening from a double clip gauge. The double clip gauges were at heights of 3mm and 6mm above the notch mouth. The double clip gauge measurements were converted to the load line displacement (LLD) by using the equation in BS7448-1 Appendix C [23]. After each test was stopped, the specimen was cooled down in liquid nitrogen and broken open, resulting in cleavage fracture. The ductile crack growth, Δa, was measured on the fracture surface of each specimen at nine equally spaced positions through the specimen thickness from the deformed notch root.

For the all specimens, the load versus the lower clip gauge extension curves are shown in Fig. 5(a) and the corresponding *J*-*R* data are shown in Fig. 5(b). Ten specimens of each notch radius were tested and interrupted at different crack extensions to generate the J-R curves. The values of *J* in Fig 5(b) were calculated from the load-LLD curve and the crack growth length using the formulae in BS7448-4 [24]. The validity of estimating *J* values for notched specimens using the method in the testing standards, developed for sharp cracks, is examined in Section 3 below.

2. Finite Element Analysis

In order to apply the ductile fracture simulations following the approach in [20], it is necessary to have descriptions of the true stress-strain behaviour of the material and the ductility as a function of

stress triaxiality. The former behaviour is derived here using the results from finite element (FE) analysis of the smooth and notched tensile tests, Section 3.1. The latter property is also derived from these same analyses, Section 3.2, with selection of the most appropriate model influenced by results from FE analyses of selected SE(B) tests. The SE(B) analyses are also used to assess the accuracy of estimating *J* for blunt notch specimens using formula in testing standards, Section 3.3.

3.1 Tensile Test Simulation

Fig. 6 shows the 2-D FE models and meshes used to simulate the smooth and notched tensile test specimens. Four-node axisymmetric linear integral element, CAX4 within ABAQUS [25] and symmetry boundary conditions were used. The minimum element size around a notch is 0.2mm. From a mesh sensitivity analysis, there were no differences in stress-strain response between 2-D and 3-D models, and for meshes with the element size around a notch ranging from 0.1mm to 0.4mm.

The true stress-strain curve of the S690 steel at 150^{o}C used for the simulations is shown in Fig 7(a). The first part of the curve was obtained from the smooth round bar test data before necking using conventional corrections to the engineering stress-strain curve. The later part of the curve was calibrated from Bridgman corrections and FE simulations of the double notched tensile tests. Fig 7(b) compares the FE load-diametral contraction curves of the double notched tensile tests with the experimental curves demonstrating the validity of the true stress-strain curve of Fig. 7(a).

3.2 Ductile Fracture Simulation for SE(B) Test

The ductile fracture simulations have followed the approach set out in [20], which is briefly described here, concentrating on calibration of the model. A stress-modified fracture strain model is constructed and used to simulate the SE(B) tests and derive resistance curves (J-R curves) for each notch root radius. The model is based on the local fracture strain being strongly dependent on the stress triaxiality, this dependence being defined by

$$\frac{\sigma_m}{\sigma_e} = \frac{\sigma_1 + \sigma_2 + \sigma_3}{3\sigma_e} \tag{1}$$

where $\sigma_{1,}\, \sigma_{2,}\, \sigma_3$ are the principal stresses, and σ_m and σ_e are the hydrostatic stress and von Mises equivalent stress. The local fracture strain, ε_f, is a function of the stress triaxiality as defined by:

$$\varepsilon_f = \alpha \exp\left(-\gamma \frac{\sigma_m}{\sigma_e}\right) + \beta \tag{2}$$

where α, β and γ are material constants which can be obtained from smooth and notched bar tensile. From the tensile test simulations described in Section 3.1, the stress triaxiality is found to generally increase with increasing equivalent plastic strain at the centre of the specimen as shown in Fig. 8(a), although for sharper notches the triaxiality is found to decrease at higher loads. In Fig. 8(b), the

fracture strain taken as the equivalent plastic strain at the failure point of each test is plotted against stress triaxiality which is taken as the average of the variation with the equivalent plastic strain from Fig. 8(a). For the applications here, three fits of the fracture model of eqn (2) are considered and the material constants for each models are summarised in Table 3. The sensitivity of the SE(B) analysis results to the choice of model is discussed in Section 4.

In the numerical analysis, incremental damage, $\Delta\omega$ is calculated at Gauss points for each increment in the analysis as:

$$\Delta\omega = \frac{\Delta\varepsilon_e^p}{\varepsilon_f} \tag{3a}$$

$$\omega = \sum \Delta\omega \tag{3b}$$

where $\Delta\varepsilon_e^p$ is the incremental equivalent plastic strain and ε_f is determined by equation (2). As the local deformation increases, the accumulated damage, ω, increases and local failure is assumed when the accumulated damage becomes unity ($\omega = 1$). Using the ABAQUS UHARD and USDFLD user-defined subroutines, all stress components are reduced to a very small value for the failed Gauss point and crack growth is simulated. For computational efficiency, the damage zone was confined to the symmetry plane containing the notch.

Fig. 9 shows the 3-D FE models for a quarter of the SE(B) specimens with five different notch root radii used in the ductile fracture simulations. Solid linear integral elements, C3D8 were used and the size of the damage element, L_e was determined to be 0.15mm from the calibration process [26-28]. The large geometry change option was used to consider the large deformation at the notch tip. Between the specimen and rigid rollers, contact conditions with no friction were applied. The displacement boundary condition was applied to a reference point of the centre roller using the MPC (multi-point constraint) option and the side roller was fixed. The reaction force and the displacement were calculated at the reference point of the centre roller to calculate *J* for the notch.

3.3 *J* Calculation for Blunt Notch

Testing standards provide methods for the measurement of the fracture toughness using various types of specimen with sharp cracks (typically fatigue pre-cracks). Here, the validity of the test methods in standards for application to blunt notches is examined. Using the results of the FE ductile fracture simulations for blunt notched SE(B) specimen, *J-R* curves are constructed from the FE domain integral method and also by applying the BS and ASTM standards to the FE load-displacement-crack growth results.

In BS 7448 [24], *J* is calculated using the load-LLD (load line displacement) curve and the initial crack length, a_o, with a correction made using the measured final crack length:

$$J=\left[\frac{PS}{BW^{1.5}}\times f\left(\frac{a_o}{W}\right)\right]\frac{(1-\nu^2)}{E}+\frac{\eta_p U_p}{B(W-a_o)}\left[1-\frac{(0.75\eta_p-1)}{(W-a_o)}\Delta a\right] \quad (4)$$

where, P is applied force, B, W and S are dimensions of specimens as shown in Fig. 4, Δa is crack growth, E and ν are elastic properties of the material, $f\left(a_o/W\right)$ is the stress intensity factor function, U_p is the plastic component of the area under the load-LLD curve and η_p is a geometric factor given in [24] which varies with type of specimen (η_p =2.0 for SE(B) specimen). From this method, a point on the *J-R* curve can be obtained from each test specimen and the results are shown in Fig. 10.

In ASTM E1820-15a [29], J is calculated using the instantaneous crack length, a_i determined during a test from the unloading compliance method or the electric potential drop method:

$$J_{(i)}=\left[\frac{P_i S}{BW^{1.5}}\times f\left(\frac{a_i}{W}\right)\right]\frac{(1-\nu^2)}{E}+J_{pl(i)} \quad (5a)$$

$$J_{pl(i)}=\left[J_{pl(i-1)}+\left(\frac{\eta_{pl}}{b_{(i-1)}}\right)\frac{A_{pl(i)}-A_{pl(i-1)}}{B}\right]\left[1-\gamma_{pl}\left(\frac{a_{(i)}-a_{(i-1)}}{b_{(i-1)}}\right)\right] \quad (5b)$$

where, A_{pl} is the area under the load-LLD record (same as U_p), b is the remaining ligament (b_i =W-a_i where a_i includes the notch radius), η_{pl} and γ_{pl} are geometric factors given in [29] which vary with type of specimen η_{pl} =1.9 and γ_{pl} =0.9 for SE(B) specimen) and other terms are the same as in BS 7448. From this method, a *J-R* curve can be obtained from each test specimen. However, here a point on a J-R curve is obtained from each test specimen with a_i taken as the crack length measured after the test.

Fig. 11 shows the FE J calculation from the domain integral method. The stress field normal to the crack face at crack initiation is shown in Fig. 11(b), where the black area denotes the region of compressive stress and the white area is the region where the equivalent stress is higher than the yield stress. When using the domain integral method, it is important to define a contour containing the stress field around the crack tip excluding the compressive area [30-31]. Fig. 11(c) shows convergence of the J values for different contours obtained from the domain integral method. The converged domain integral values of J are plotted with the J values from the BS and ASTM standard methods for three different notch radii in Fig. 10. Here, converged values are the computed value of J that have reached a saturated value, obtained in the "far-field" remote from the crack tip, averaged through the thickness. The contours were chosen to be sufficiently far away from the crack tip to surround the plastic zone and pass through the elastic region only, including the whole stress fields produced by the presence of the notch, but close enough to avoid any errors resulting from the influence of specimen boundaries. In damage simulations, J is evaluated in each calculation step after taking the stiffness of the integration points with ω =1 as zero. This ensures path independency. The ASTM method shows good agreement with the domain integral method for all cases, but for the BS method, the difference increases with increasing notch root radius. Therefore, in subsequent

comparisons, experimental *J-R* curves are taken as those obtained from the tests using estimates of *J* using the ASTM formula. The corresponding estimates of crack growth are evaluated using the 9-point average approach used to interpret the experimental results.

4. Damage Analysis Results

In this section, ductile fracture simulation results are presented for the SE(B) tests for the five different notch radii tested. The sensitivity of the results to the selection of the fracture criterion, shown in Fig. 8(b), is presented in terms of comparisons of the load versus displacement curves and the crack growth versus displacement curves with test data. From the sensitivity analyses, the effects of the fracture model on the ductile crack initiation and growth results from the sharp to the most blunt notch geometry are analysed. Finally, the *J-R* curves for the notches are constructed by using criterion 3 in Fig. 8(b), which gives the best agreement with the experimental data for all notches. From the *J-R* curves, the effective initiation fracture toughness values, J_{IC}^{ρ}, for the notches are determined and the fracture ratio, K_r, required in Failure Assessment Diagram (FAD) assessments is calculated.

4.1 Load-Load Line Displacement Data

Fig. 12 shows the load-LLD results from the analyses for the five different notch radii for the three fracture criteria. For the sharp notch (ρ = 0.15mm), there is little difference between results using the different criteria, and the analyses are in good agreement with the observed experimental response. As the notch radius increases, the difference between the analyses with different fracture criteria is larger but good agreement with the experimental data remains up to approximately the maximum load. The constraint at the notch tip, i.e. the stress triaxiality, decreases with increasing notch radius. The fracture strain at lower stress triaxiality is lower with the fit of criterion 3 than for criteria 1 and 2, as shown in Fig. 8(b), and this appears to give more conservative predictions of load in Fig.12.

4.2 Crack Growth-Load Line Displacement Data

Fig. 13 shows the crack growth-LLD results from the analyses for the five different notch radii. Fig. 13(a) compares the results the sharp notch (ρ = 0.15mm) for the three fracture criteria. The slope of the curve resulting from use of criterion 1 is much higher than that of the test data whereas the results from application of criteria 2 and 3 provide more realistic slopes. From the studies, it was found that the material constant, β in eqn (2), affects the slope and the value β = 0.25 was found to be satisfactory. The crack growth-LLD results for all notch radii are presented in Fig 13(b), 13(c) and 13(d), for criteria 1-3, respectively. For the blunt notches, criterion 3 showed better agreement with test data than criterion 2.

4.3 *J-R* Curves and Determination of Fracture Toughness for Blunt Notch

From the above analysis, *J-R* curves have been constructed from the FE results obtained using the fracture criterion 3 by applying the ASTM E1820-13 approach [29]. Fig. 14(a) compares the FE *J-R*

curves for all notches with the test data. The results from the ductile damage simulations provide good prediction of the experimental *J-R* curves for the wide range of notch geometry.

Effective initiation fracture toughness values for the notches, $J^{\rho}_{0.2}$, have been defined by the *J* value at 0.2mm crack growth according to the ESIS procedure [32]. In the current work, $J^{\rho}_{0.2}$ values were normalised by $J^{\rho=0.15}_{0.2}$ as no pre-cracked specimen data were available. Fig. 14(b) shows the results in terms of the normalised value, $J^{\rho}_{0.2}/J^{\rho=0.15}_{0.2}$; a linear increase of this ratio with notch radius is apparent. Similar approximately linear increases were found for a range of materials in [20] and this is discussed further in Section 5.

4.4 Failure Assessment Diagram Analysis

In [20], it was shown that as the notch radius becomes larger for defects in compact tension specimens, assessment points on a FAD are shifted downwards so that failure tends to towards collapse dominated rather than fracture dominated. Similar assessments are performed for the notched SE(B) specimens and this requires the fracture ratio K_r and the plastic collapse ratio L_r which are defined as [3]:

$$K_r = \frac{K^{\rho}_I}{K^{\rho}_{mat}} = \sqrt{\frac{J^{\rho}_{el}}{J^{\rho}_{0.2}}} \quad \text{for blunt defects} \tag{6a}$$

$$L_r = \frac{P}{P_L(\sigma_{YS},\, a,\, \rho)} \tag{6b}$$

where K^{ρ}_I, K^{ρ}_{mat}, J^{ρ}_{el} and $J^{\rho}_{0.2}$ are the stress intensity factor, fracture toughness, elastic *J* and initiation toughness for a blunt notch, respectively and *P*, P_L, σ_{YS}, *a* and ρ are the applied load, limit load, 0.2% proof stress, crack size and notch radius, respectively.

From the ductile fracture simulation results leading to the fracture toughness in Fig. 14, the values of fracture ratio, K_r were calculated for each notch radius. The elastic *J* for notches, J^{ρ}_{el} was obtained using the stress intensity factor solution in ASTM E1820-15a, as given in the first part of eqn (5a), and the fracture toughness values, $J^{\rho}_{0.2}$ were defined by the *J* value at 0.2mm crack growth as shown in Fig. 14(a).

To calculate the plastic collapse ratio L_r, 3-D elastic-perfectly-plastic analyses for a material with a yield stress of 423.4MPa were performed with a geometrically linear analysis for the five notch radii. The limit loads for the notch radii were obtained by using the twice-elastic slope (TES) method (see, for example, [33]), although the resulting collapse loads are not sensitive to the method adopted as a perfectly plastic material model was used. The collapse loads are summarized in Table 4 and reduce with increasing notch radius. Also given in the table is the R6 solution [3] for a 2-D cracked SE(B) specimen in plane strain and this is conservative (lower) relative to the 3-D FE result.

Fig. 15 shows the FAD assessments for the SE(B) tests with the five notch radii. The Option 1 FAD curve in R6 [3] was constructed as the failure assessment curve with the plastic collapse cut-off defined from the tensile properties for modified S690 steel at 150°C. The value of K_r increases linearly with increasing L_r for the all notch radii as both are directly proportional to load. The value of K_r decreases as the notch radius increases for the same L_r. Hence, crack initiation becomes more collapse dominated with increasing notch bluntness. However, crack initiation is predicted to occur beyond plastic collapse line for the all notch radii, consistent with the experimental data.

5. Discussion

Both the experimental and FE simulated J-R curves have been presented in terms of the average crack extension. However, crack growth was not uniform through the specimen thickness. For the tests, information on the non-uniformity is available from the fracture surfaces. As the FE analyses were performed in 3-D, these also lead to non-uniform crack extension due to variations in crack driving force (J) and stress triaxiality through the section. Some comparisons of the experimental and simulated crack growth are shown in Fig. 16, both being crack growth on the symmetry plane. As the notch radius increases, the degree of non-uniform crack growth increases such that crack growth only occurs in the centre portion of the specimens with the wider notches. It can be seen that not only has the global fracture response been well simulated by the ductile damage modelling, Fig. 14, but also from Fig. 16 that the local fracture behaviour through the thickness has been well modelled. This gives added confidence in the ability of the ductile fracture approach to simulate real component behaviour.

For the specimens reported in this paper, all photographs were taken looking down onto the cleavage fracture surface which was approximately aligned with the symmetry plane; no study was undertaken into potential deviations of tearing away from the symmetry plane for these specimens. However, such a study was undertaken for other specimens tested at +50°C with ρ=1.2mm. After loading beyond maximum load, each specimen was sectioned along the centre-line to show the extent of tearing at the specimen centre (these specimens were neither cooled in liquid nitrogen nor broken open). Three key observations could be made:

- Tearing away from the symmetry plane (zig-zag pattern) occurred at small Δa.
- Tearing in a straight line (parallel to symmetry plane) occurred at large Δa (once the crack tip is sufficiently ahead of the notch tip).
- More than one ductile tear initiated in some cases.

Based on the above observations, ductile tearing from notch tips is more complex than from fatigue pre-cracks. The definition of an appropriate value of crack growth is therefore not as straightforward for notched specimens, especially early in the tearing process where multiple short ductile tears may be in competition with each other on different planes. This also makes the corresponding measurement of Δa more challenging when a specimen is broken open after a test: the full extent of ductile tearing may not be visible on the final fracture surface, and some ductile tearing may be hidden from view on planes other than the visible fracture surface. The approach taken in this paper to define and measure an average Δa on the symmetry plane in both the experimental measurements

and numerical analyses is a simple and convenient method for making comparisons. However, further consideration of how to undertake experimental measurement of the extent of ductile tearing from a notch is likely to be required if notch J-R curves are to be used in defect assessments. Modelling approaches, such as that used in this paper, could aid the development of such test guidance.

In calibrating the ductile fracture model, three different models were considered, as shown in Fig. 8(b). This was because only overall extension data rather than reduction of area data were available from the smooth tensile tests, making it difficult to provide an accurate fit at low triaxiality, and notched specimen tests did not lead to triaxiality as high as near the crack or notch tip in fracture tests, making it difficult to provide an accurate fit at high triaxiality. This suggests that smooth tensile tests should be performed with diametral extensometry and notched bar tensile tests should be performed with a range of notch shapes in order to calibrate the ductile damage model. However, for the current analyses, it was found that the calibration could be guided by the ductile fracture data from the SE(B) tests with acute notches, leading to successful simulation of the blunt notched specimens, Figs 14 and 16.

In practice, ductile fracture simulations are expensive to perform and therefore, as noted in the Introduction, a number of authors have proposed simple fits to describe the effect of notch radius on fracture toughness. For example, Horn and Sherry [18], from Weibull stress analysis and cleavage fracture test results, have suggested that the increase in effective fracture toughness may be described for the SE(B) and C(T) specimens by:

$$\frac{K_{mat}^{\rho}}{K_{mat}} = 1 + \phi \left(\frac{\sigma_N}{\sigma_y} \right)^{-\ell}$$

$$\sigma_N = \frac{3PS}{2BW^2} \left(1 + 2Y \sqrt{\frac{a}{\rho}} \right) \qquad \text{SE(B) specimen} \qquad (7)$$

$$\sigma_N = \frac{P}{B(W-a)} \left(1 + 2Y \sqrt{\frac{a}{\rho}} \right) \qquad \text{C(T) specimen}$$

where K_{mat}^{ρ} is the notch fracture toughness for a blunt notch (the stress intensity factor equivalent of $J_{0.2}^{\rho}$), the elastic notch stress σ_N is defined by the normalised stress intensity factor function, Y, and ϕ, ℓ are fitting constants, dependent on material and temperature.

The ability of eqn (7) to fit ductile fracture data has been explored by application to both the results of the fracture simulations in [20] and those in this paper for the modified S690 steel. Results are shown in Fig. 17. The constants used to fit the initiation fracture toughness data are given in Fig. 17 and the ratio of effective notch toughness to sharp crack toughness in Fig. 17(a) as a function of normalised elastic notch stress and in Fig. 17(b) as a function of notch radius. It can be seen that the approach of eqn (7), although developed to describe cleavage fracture, also works well for ductile fracture and therefore may be suitable as a general description of the effect of notch radius on

fracture toughness. It can also be seen that for the materials examined, there is an approximately linear increase in effective fracture toughness with notch radius.

6. CONCLUSIONS

Smooth tensile, notched bar tensile and multi-specimen single edge notched bend tests with various notch acuities have been performed and show an increase in effective ductile fracture toughness with increasing notch radius. The data have been fitted with a ductile fracture model, which has been shown to be capable of predicting the global deformation and fracture response as well as the local variation of ductile crack extension through the thickness. The influence of notch radius on fracture assessment has been discussed and assessments have been shown to become more collapse dominated with increasing notch bluntness. Finally, an empirical fit developed to describe the effect of notch radius on cleavage fracture toughness has been examined and found to be also capable of describing the effect of notch radius on ductile fracture toughness.

ACKNOWLEDGEMENTS

The release of ductile fracture data by Tata Steel through Mr Adam Bannister is gratefully acknowledged, as are helpful discussions with the members of the R6 Panel. The authors would like to acknowledge the funding and technical support from BP through the BP International Centre for Advanced Materials (BP-ICAM) which made this research possible.

REFERENCES

[1] American Petroleum Institute/ American Society of Mechanical Engineers, API 579/ASME FFS-1, Recommended practice for fitness-for-service, API; 2016.

[2] BS 7910:2013+A1:2015, Guide to methods for assessing the acceptability of flaws in metallic structures. British Standard Institution, London, UK; Incorporating Corrigenda 1 and 2, 2016.

[3] R6, Revision 4, with updates to Amendment 11, Assessment of the integrity of structures containing defects. EDF Energy, Gloucester, UK; 2015.

[4] EGIG-group, Gas Pipeline Incidents, 8th Report of the European Pipeline Incident Data Group (document number EGIG 11.R.0402); 2011.

[5] Pluvinage G, Allouti M, Schmitt C and Capelle J. Assessment of a gouge, a dent, or a dent plus a gouge, in a pipe using limit analysis or notch fracture mechanics, Journal of Pipeline Engineering 2011;10:147-160.

[6] Kim JH, Kim DH and Moon SI, Evaluation of static and dynamic fracture toughness using apparent fracture toughness of notched specimen. Materials Science and Engineering A. 2004;387:381-4.

[7] Livieri P, Use of J-integral to predict static failures in sharp V-notches and rounded U-notches. Engng Fract Mech 2008;75:1779-93.

[8] Yoda M. The effect of the notch root radius on the J-integral fracture toughness under modes I, II and III loadings. Engng Fract Mech 1987;26:425-31.

[9] Faucher B, Tyson W, Hong Y and Boutin J, Dependence of ductile fracture toughness of a weld metal on notch root radius and inclusion content, Int J Fract 1990;46:173-84.

[10] Kamat S and Srinivas M, Investigation of blunting line and evaluation of fracture toughness under mixed mode I/III loading in commercially pure titanium. Materials Science and Technology 2003;19:62-6,

[11] Susmel L and Taylor D, On the use of the Theory of Critical Distances to predict static failures in ductile metallic materials containing different geometrical features, Engng Fract Mech 2008;75:4410-21.

[12] Milne I, Chell G and Worthington P, The mechanisms of fracture in blunt-notched specimens of a low alloy steel and the effect on failure assessment. Materials Science and Engineering 1979;40:145-57.

[13] Suo Z, Ho S and Gong X. Notch ductile-to-brittle transition due to localized inelastic band. Journal of Engineering Materials and Technology 1993;115:319-26.

[14] Cicero S, Gutiérrez-Solana F and Horn AJ. Experimental analysis of differences in mechanical behaviour of cracked and notched specimens in a ferritic–pearlitic steel: Considerations about the notch effect on structural integrity. Engng Failure Analysis 2009;16:2450-66.

[15] Matvienko YG and Morozov E. Calculation of the energy J-integral for bodies with notches and cracks. Int J Fract 2004;125:249-61.

[16] Taylor D, Cornetti P and Pugno N. The fracture mechanics of finite crack extension. Engng Fract Mech 2005;72:1021-38.

[17] Cicero S, Gutiérrez-Solana F and Álvarez J. Structural integrity assessment of components subjected to low constraint conditions. Engng Fract Mech 2008;75:3038-59.

[18] Horn A and Sherry A. An engineering assessment methodology for non-sharp defects in steel structures–part I: procedure development. Int J Pres Ves Piping. 2012;89:137-50.

[19] Horn A and Sherry A. An engineering assessment methodology for non-sharp defects in steel structures–Part II: Procedure validation and constraint analysis. Int J Pres Ves Piping. 2012;89:151-61.

[20] Han J-J, Larrosa N O, Kim Y-J and Ainsworth R A. Blunt Defect Assessment in the Framework of the Failure Assessment Diagram. Int J Pres Ves Piping 2016;146:39-54.

[21] Larrosa N.O and Ainsworth R.A. Ductile fracture modelling and J-Q fracture mechanics: a constraint based fracture assessment approach. Frattura ed Integrita Strutturale, 2016; 38, 266-72

[22] ASTM E8/E8M, Standard Test Methods for Tension Testing of Metallic Materials, Book of Standards Volume: 03.01, ASTM International, USA.

[23] BS 7448-1:1991, Fracture mechanics toughness tests. Method for determination of K_{Ic}, critical CTOD and critical J values of metallic materials, BSi, UK.

[24] BS7448-4:1997, Fracture mechanics toughness tests. Method for determination of fracture resistance curves and initiation values for stable crack extension in metallic materials, BSi, UK.

[25] ABAQUS version 6. 13, 2013, User's manual, Inc. and Dassault Systems.

[26] Oh C-S, Kim N-H, Kim Y-J, Baek J-H, Kim Y-P, Kim W-S. A finite element ductile failure simulation method using stress-modified fracture strain model. Engng Fract Mech 2011;78:124-37

[27] Kim N-H, Oh C-S, Kim Y-J, Yoon K-B, Ma Y-H. Comparison of fracture strain based ductile failure simulation with experimental results. Int J Pres Ves Piping 2011;88:434-47.

[28] Jeon J-Y, Kim N-H, Kim Y-J, Lee S-Y, Kim J-W. Predictions of Mechanical Properties From Small Punch Test Results Using FE Damage Analyses. ASME 2013 Pressure Vessels and Piping Conference: American Society of Mechanical Engineers; 2013.

[29] ASTM E1820-15a, Standard Test Method for Measurement of Fracture Toughness, Book of Standards Volume: 03.01, ASTM International, USA.

[30] Østby E, Thaulow C, Zhang ZL. Numerical simulations of specimen size and mismatch effects in ductile crack growth – Part I: Tearing resistance and crack growth paths. Engng Fract Mech 2007;74:1770-92.

[31] Brocks W, Anuschewski P, Scheider I. Ductile tearing resistance of metal sheets. Engineering Failure Analysis. 2010;17:607-16.

[32] ESIS P2-92: ESIS procedure for determining the fracture behaviour of materials; 1992.

[33] Seal C K, Han J -J and Ainsworth R A, A comparison of various plastic work curvature methods, Int J Pres Ves Piping. 2015;135-136:26-35.

Table 1. Summary of tests for modified S690 steel at 150°C

Test	Geometry of specimen	Specimen number
Tensile test	Smooth round bar	E20, E21
	Double notched bar (R=1.2mm)	H1, H2, H3
	Double notched bar (R=2.0mm)	H4, H5, H6
	Double notched bar (R=6.4mm)	H7, H8, H9
SE(B) test	Single notch (ρ=0.15mm)	F24~F33
	Single notch (ρ=0.25mm)	F58~F67
	Single notch (ρ=0.75mm)	F79~F82, F95~F100
	Single notch (ρ=1.2mm)	F135~F144
	Single notch (ρ=2.0mm)	F145~F154

Table 2. Tensile properties of modified S690 steel at 150°C

Elastic modulus (GPa)	Yield stress (MPa)	Tensile stress (MPa)
180.8	423.4	609.3

Table 3. Material constants of fracture models

	α	β	γ
Criterion 1	1.78	0.0	1.34
Criterion 2	2.1	0.25	2.5
Criterion 3	1.8	0.25	2.5

Table 4. Limit load for notch radius

ρ (mm)	P_L (kN)
R6 solution	5.92
0.15	6.41
0.25	6.36
0.75	6.16
1.2	5.85
2	5.70

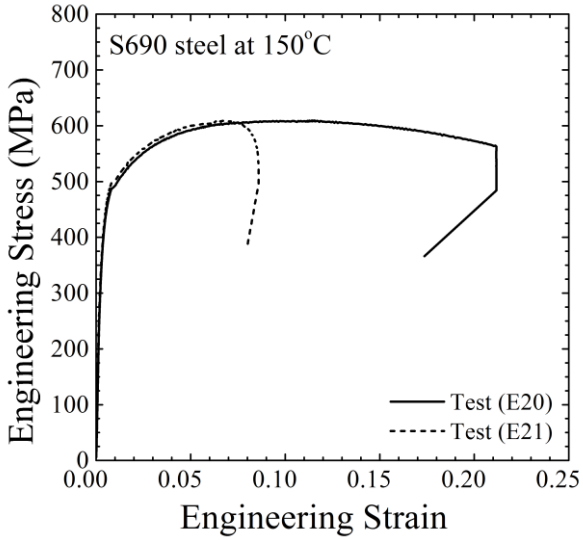

Fig. 1. Engineering stress-strain curves of modified S690 steel at 150°C

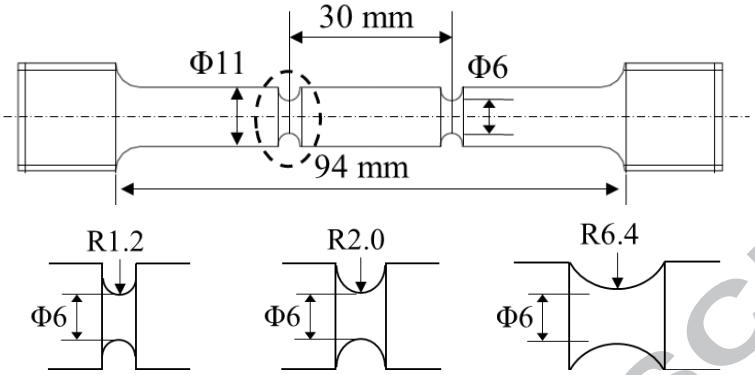

Fig. 2. Geometry of double notched tensile specimens.

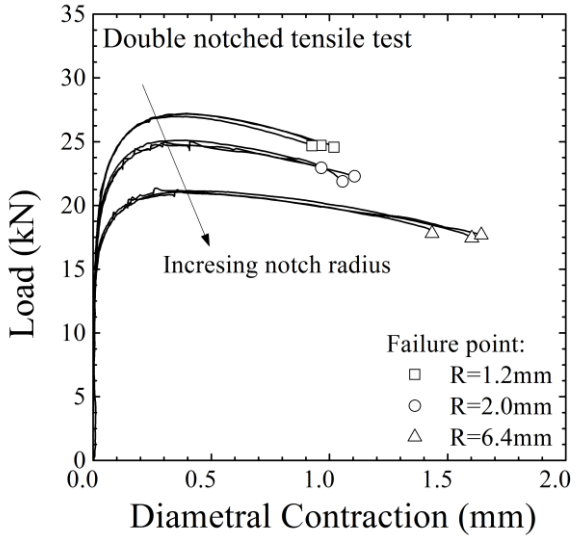

Fig. 3. Load-diametral contraction curves of double notched tensile specimens

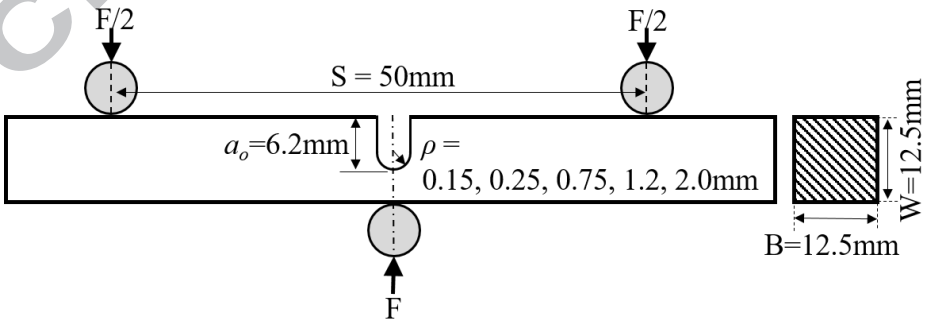

Fig. 4. Geometry of 3-point bend test and SE(B) specimens.

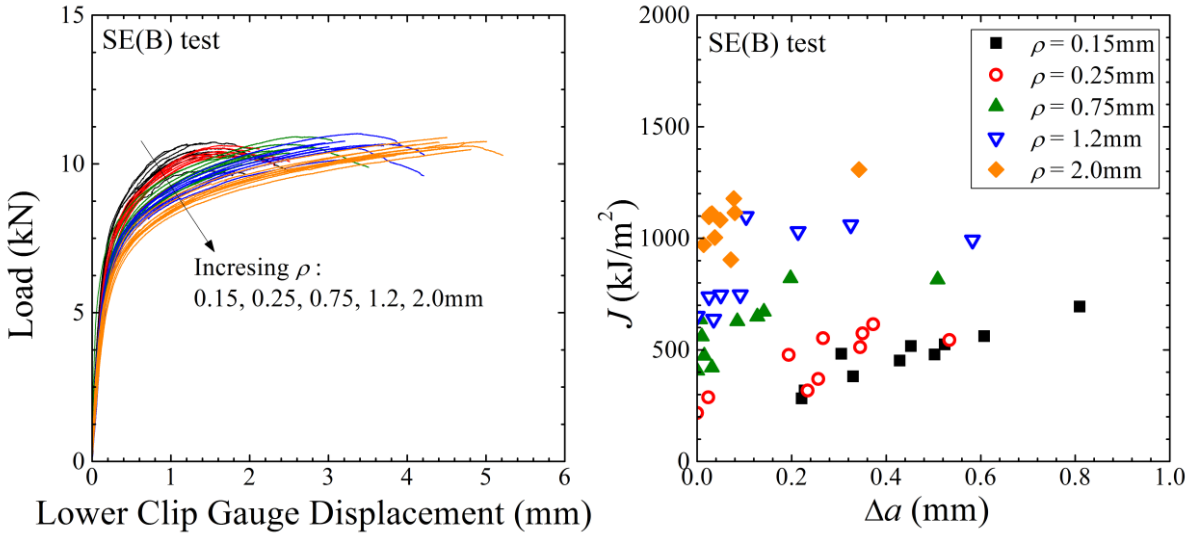

(a) (b)

Fig. 5. SE(B) test data from each specimen: (a) load vs. lower clip gauge and (b) J-R data.

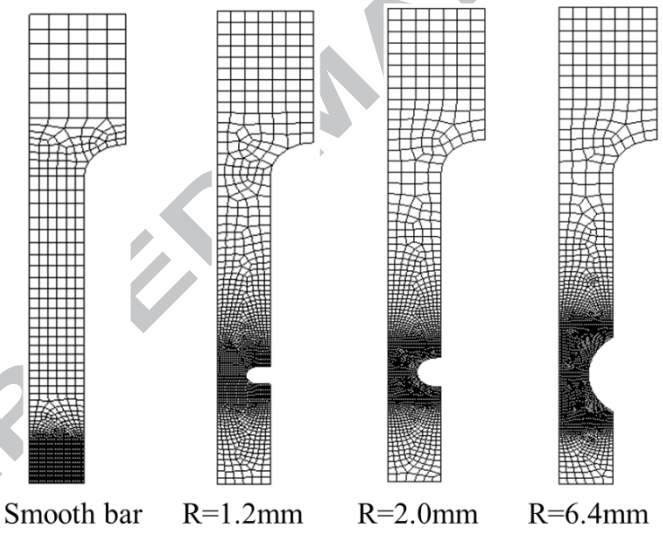

Fig. 6. Finite element model for smooth and double notched tensile test specimens

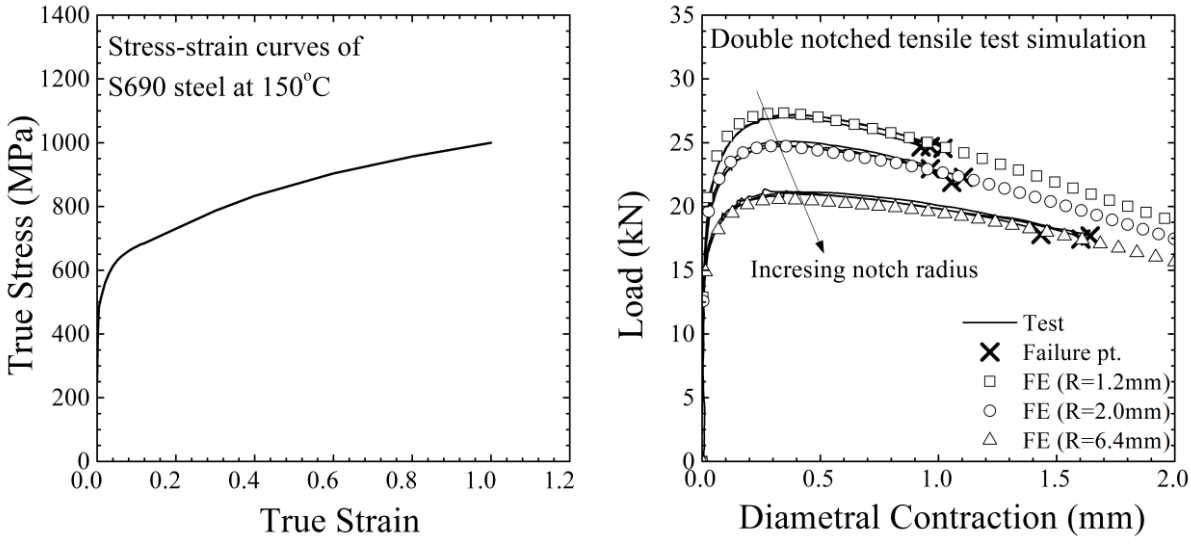

(a) (b)

Fig. 7. (a) True stress-strain curve of modified S690 steel at 150°C and (b) double notched tensile test simulation results.

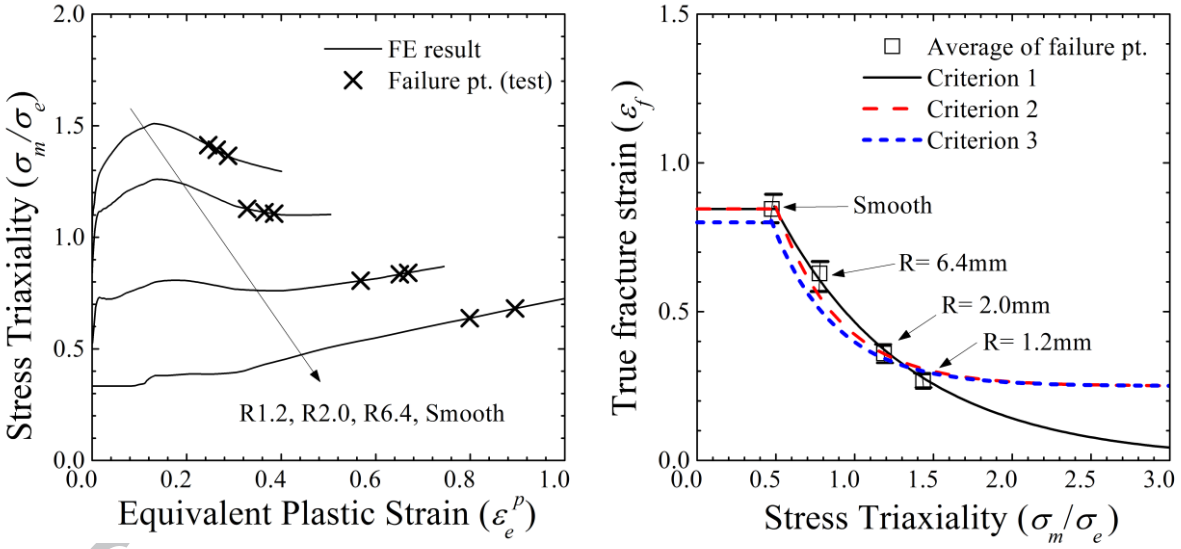

(a) (b)

Fig. 8. (a) Variations of stress triaxiality with equivalent plastic strain for smooth and notched tensile specimens and (b) the stress-modified fracture strains for modified S690 steel at 150°C.

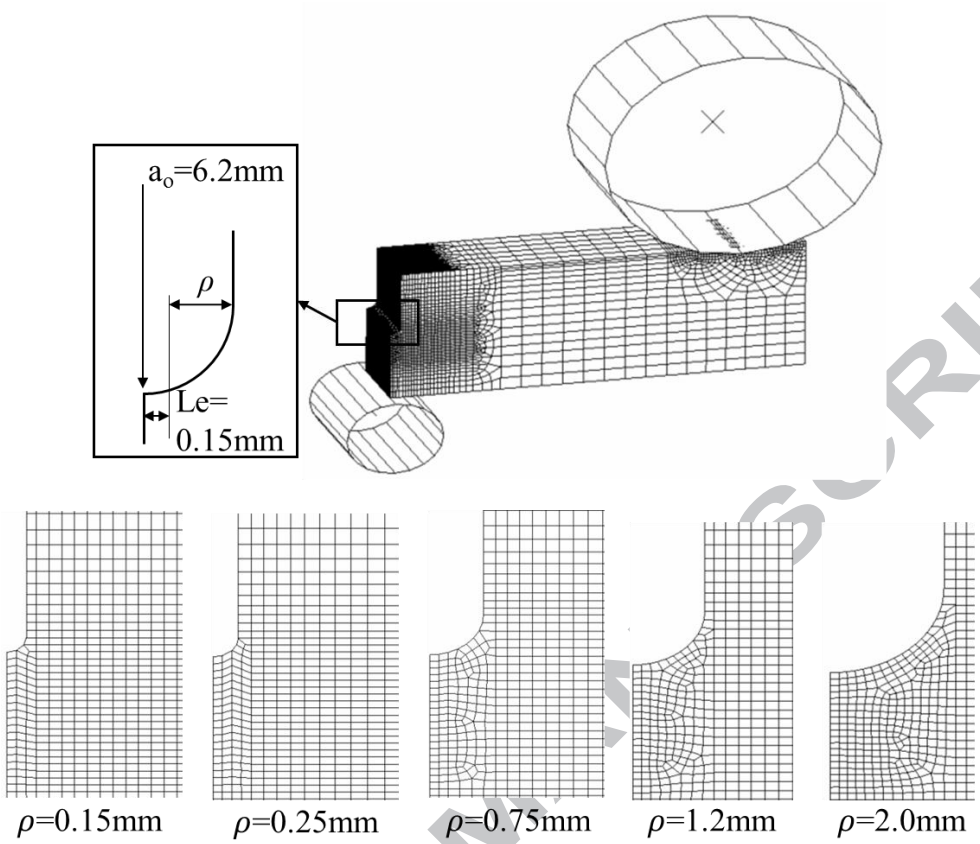

Fig. 9. Finite element model for SE(B) test specimens with 5 different notch radii.

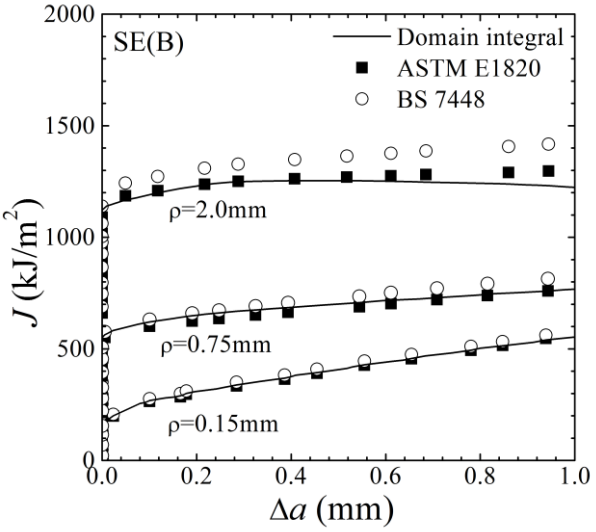

Fig. 10. Comparison of J value between ASTM E1820, BS 7448 and domain integral.

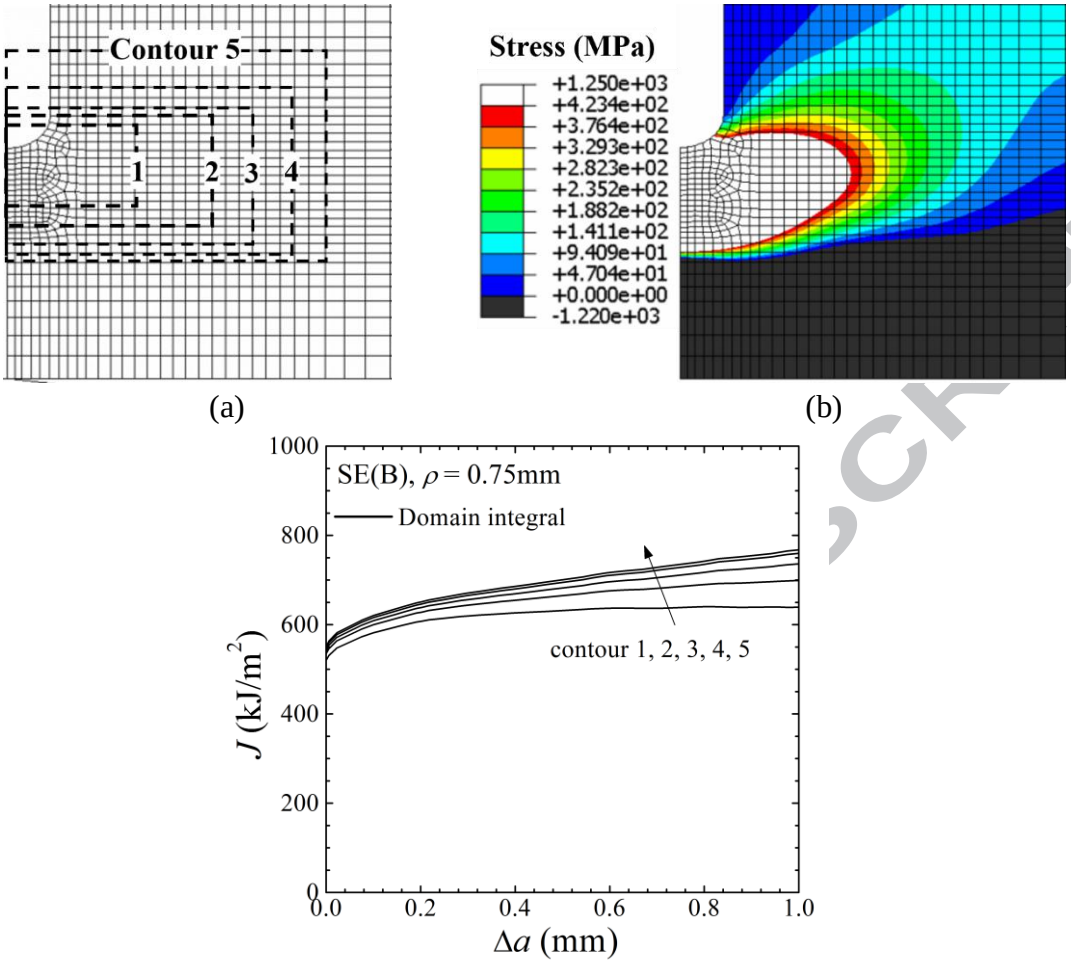

Fig. 11. Domain integral J from damage FE analysis for ρ=0.75mm: (a) contours, (b) stress field (normal to crack face) at crack initiation and (c) domain integral J-R curves.

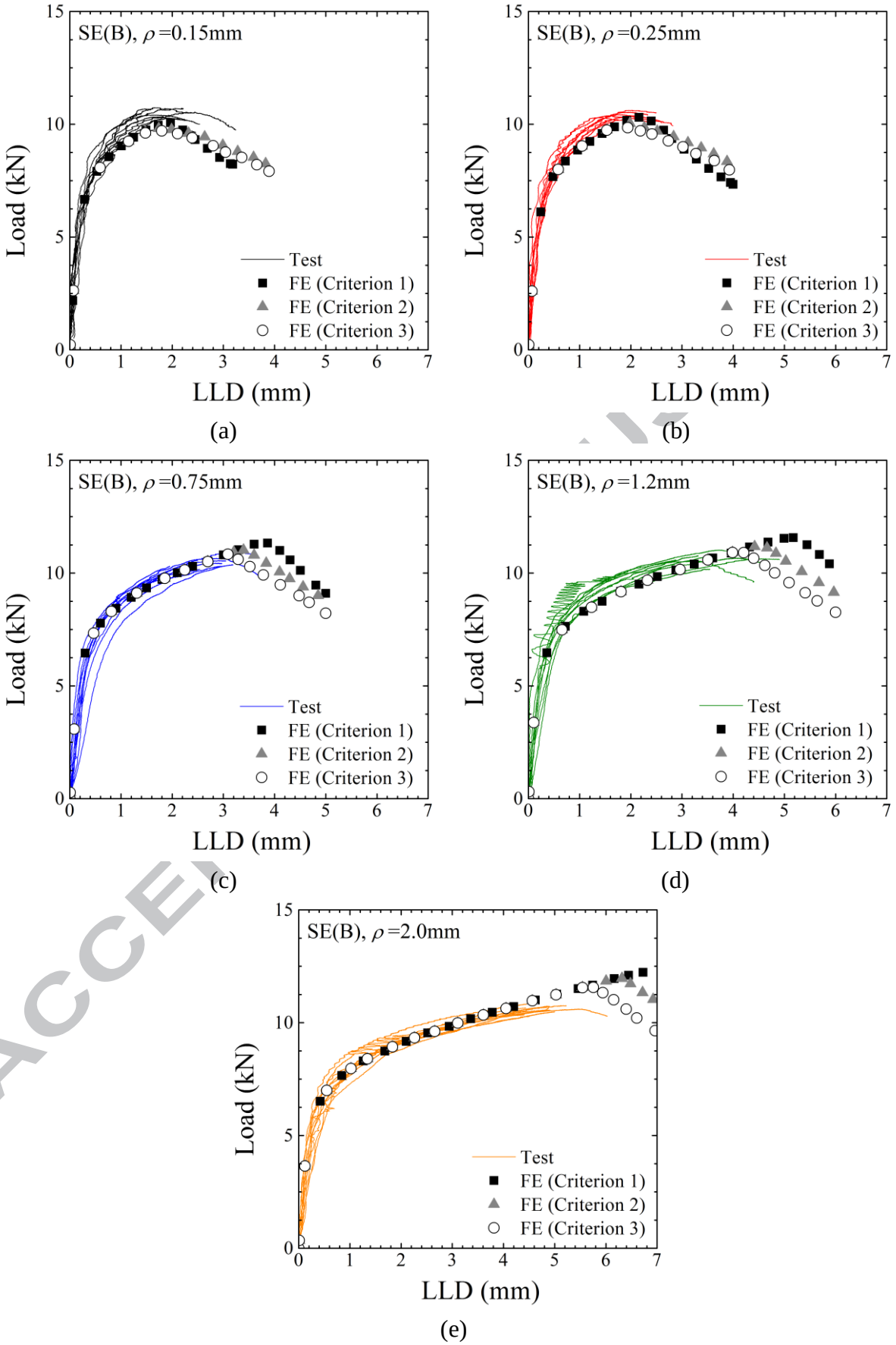

Fig. 12. Comparison of FE simulations of load-LLD curves with those from the SE(B) tests

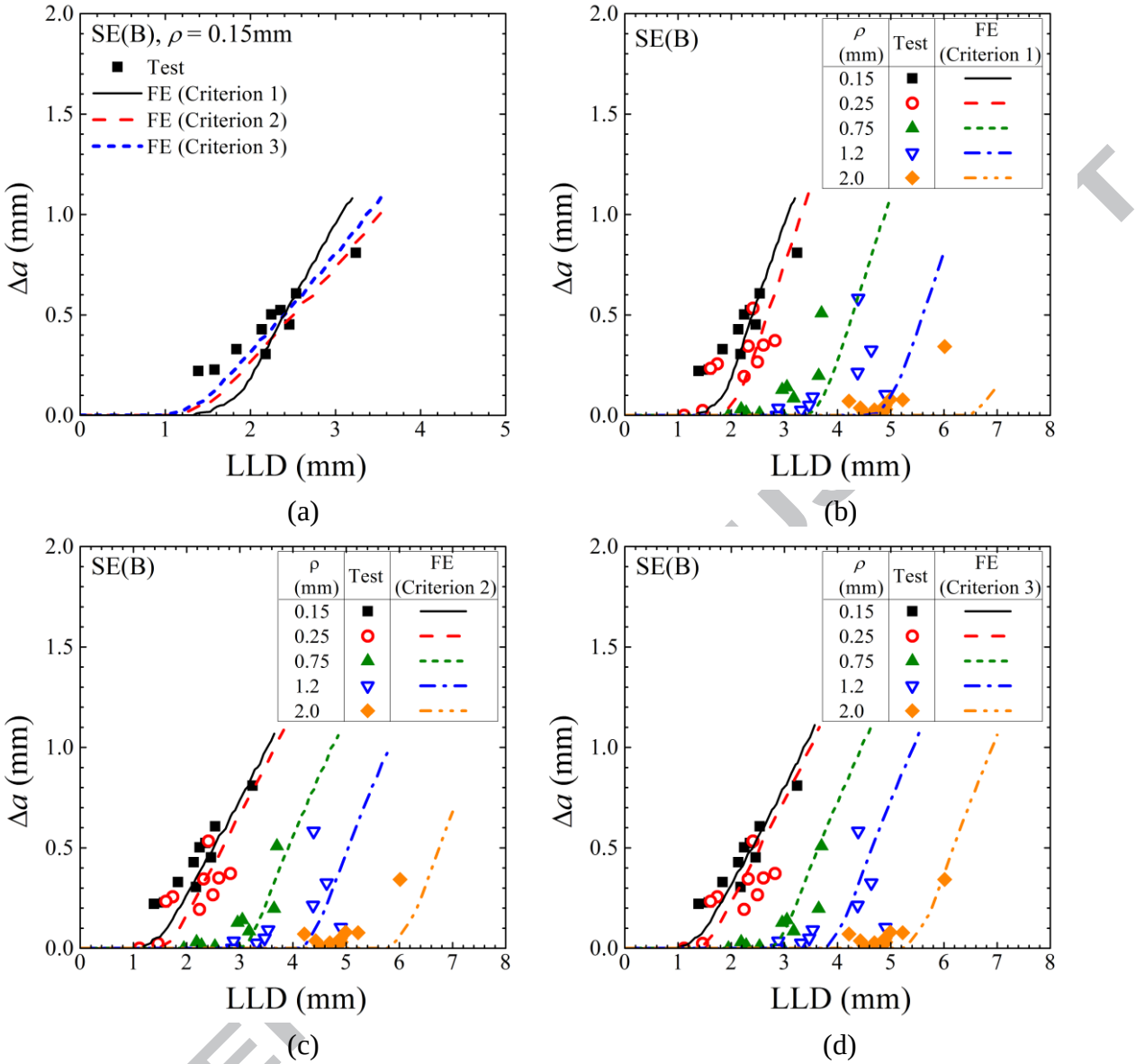

Fig. 13. Comparison of FE simulations of crack growth-LLD curves with those from SE(B) tests

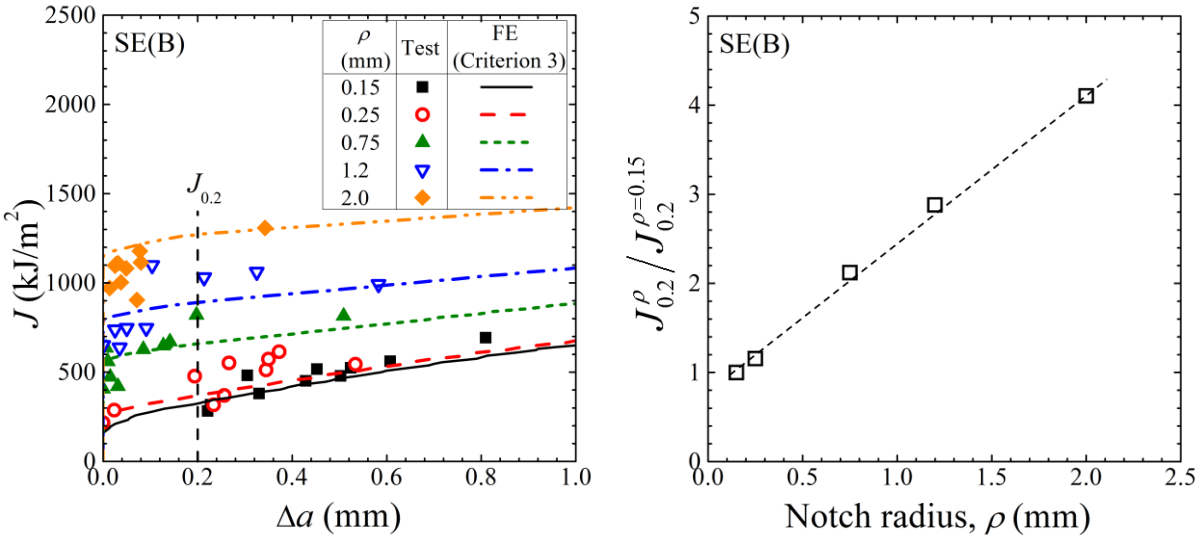

(a) (b)

Fig. 14. Comparison of FE results with experimental J-R data from SE(B) tests: (a) determination of effective initiation toughness and (b) normalised effective initiation toughness as function of notch radius.

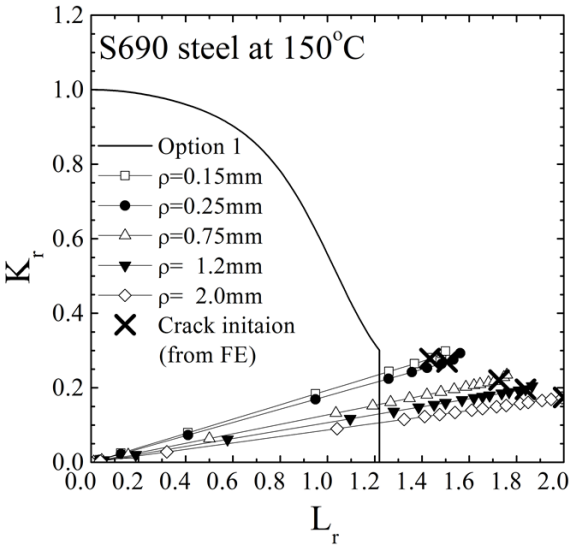

Fig. 15. FAD assessment with increasing load for SE(B) test with 5 different notch radii

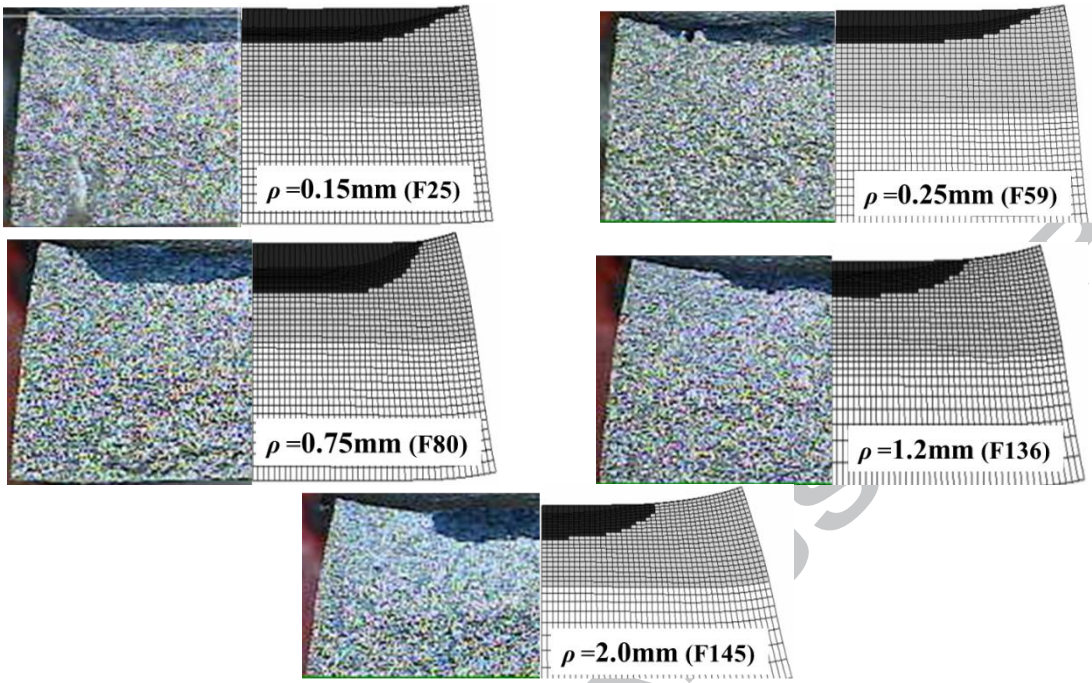

Fig. 16. Comparison of fracture surface for SE(B) test specimens with 5 different notch radii.

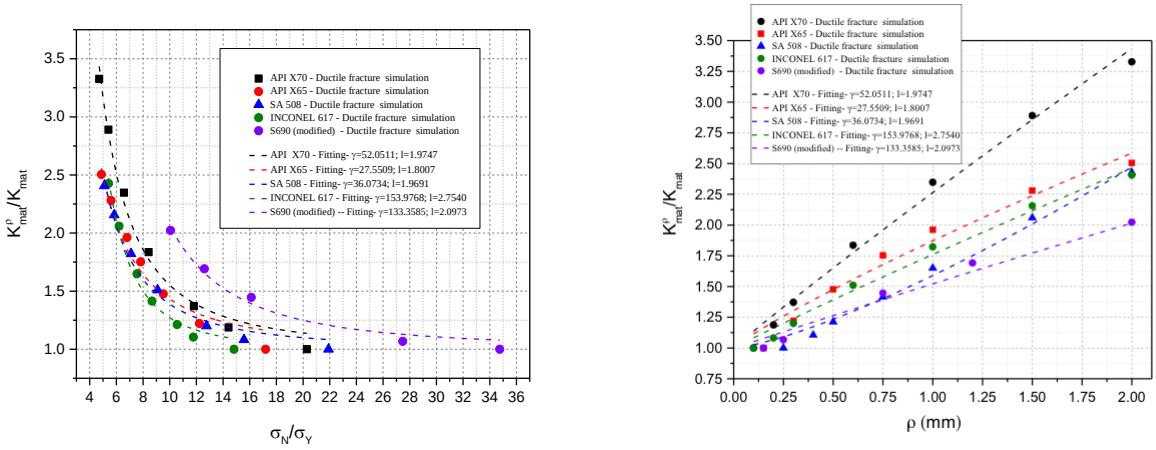

(a) **(b)**

Fig. 17 Comparison of the results of the ductile fracture simulations in [20] and in this paper with the model of Horn and Sherry [18]; (a) in terms of notch stress, (b) as a function of notch root radius

Highlights:

- Notch acuity effect has been assessed for modified S690 steel in the ductile regime.
- Results showed an increase in fracture toughness with increasing notch radius.
- Tests of notch bend specimens were used to validate ductile fracture simulations.
- Fracture simulations captured the through-the-thickness 3D nature of crack growth.
- An empirical fit for cleavage fracture was found to be useful on ductile regime.